Sensors and Actuators B 254 (2018) 681–689

Contents lists available at ScienceDirect

Sensors and Actuators B: Chemical

journal homepage: www.elsevier.com/locate/snb

Tuning the visible photoluminescence in Al doped ZnO thin film and its application in label-free glucose detection

Joydip Ghosh [a], Ramesh Ghosh [a,b], P.K. Giri [a,b,*]

[a] Department of Physics, Indian Institute of Technology Guwahati, Guwahati 781039, India
[b] Center for Nanotechnology, Indian Institute of Technology Guwahati, Guwahati 781039, India

ARTICLE INFO

Article history:
Received 9 May 2017
Received in revised form 13 July 2017
Accepted 14 July 2017
Available online 17 July 2017

Keywords:
Al doped ZnO
Photoluminescence quenching
Glucose sensor
Electron transfer
Stern-Volmer plot

ABSTRACT

Herein, we study the effect of thermal annealing on the structural and optical properties of Al doped ZnO (AZO) thin film and its application for the label-free detection of glucose based on fluorescence quenching. AZO thin films grown by radio frequency magnetron sputtering are annealed at different temperatures (250–650 °C) in air environment. The post-growth annealing improves the structural quality of the AZO films, as confirmed from the X-ray diffraction, X-ray photoelectron spectroscopy and micro-Raman analyses. The as-grown and annealed samples show strong photoluminescence (PL) in the UV (~3.33 eV) and visible-NIR (1.6–2.2 eV). The UV PL peak is originated from the near band edge emission of crystalline ZnO, while the broad visible-NIR PL is associated with the radiative transition related to oxygen interstitial (O_i) defects in the ZnO structure. The PL peak intensity is strongly enhanced after annealing due to the partial removal of non-radiative defects. The high intensity visible-NIR PL of the annealed samples is used for the label-free enzyme-based detection of glucose with the help of glucose oxidase based on PL quenching via electron transfer mechanism. Our AZO thin films can efficiently detect ~20 μM concentration of glucose in presence of glucose oxidase (GOx). We have attempted to quantify the nature of PL quenching based on the Stern-Volmer plot and explained the quenching mechanism as collisional quenching due to charge transfer in presence of a quencher. The Stern-Volmer plot of PL quenching of AZO thin film reveals the linear relationship between the quenching effect and the glucose concentration. Higher sensitivity of the sensor can be achieved by tuning the structure and doping density of the AZO films. This report opens up avenues for the non-destructive, label-free detection of biomolecules with high sensitivity using a low cost ZnO thin film.

1. Introduction

In last few decades, metal oxide thin films and nanostructures have drawn enormous attention due to their unique physical and chemical properties, and wide range of applications in different areas of nanotechnology. Among others, ZnO nanostructure has emerged as key player due to its high abundance, cheap fabrication process, chemical/thermal stability, non-toxicity, excellent radiation hardness, low electrical resistivity (ρ) of ~10^{-4} Ω-cm, a wide band gap (E_g) of 3.36 eV, a large exciton binding energy of 60 meV and high transparency at room temperature (RT) [1]. ZnO thin films are extensively studied due to its ease of synthesis, fascinating properties and a wide range of applications, such as solar cells [2], LEDs [3], photodetectors [4,5], FET [6], artificial photosynthesis, photocatalysis[7] etc [8]. ZnO and AZO thin films have been extensively used in different type of sensing applications, such as gas sensing [9–12], bio sensing [13–15] and UV detection [16]. In order to improve the electrical and the photophysical properties of ZnO, a variety of group II or III elements, such as Mg, B, Ga, In, and Al are used as appropriate dopants [17–19]. Besides inorganic materials, polymer and organic molecules can be doped in ZnO to tune its optical properties for various applications [20–22]. Al doped ZnO has better thermal, chemical and mechanical stability, non-toxicity, enhanced electrical conductivity due to the increase in free carrier concentration. Its good optical transparency make it a promising candidate as an alternative of costly Indium Tin oxide (ITO) in thin-film photovoltaic applications [11]. The physical properties of thin films mainly depend on the preparation method and the process parameters. A lot of methodologies have been developed for the growth of high quality AZO thin films, such as spray pyrolysis, hydrothermal, thermal evaporation and sputtering

* Corresponding author at: Department of Physics, Indian Institute of Technology Guwahati, Guwahati, 781039, India.
E-mail address: giri@iitg.ernet.in (P.K. Giri).

http://dx.doi.org/10.1016/j.snb.2017.07.110
0925-4005/

methods [23–25]. Among these, the magnetron sputtering method is widely used, since it provides film with high surface uniformity, high packing density and strong adherence to the substrate at a high deposition rate to prevent interfacial degradation in devices [26,27]. AZO thin film shows excellent transparency in the visible range and high intensity photoluminescence (PL), which is usually composed of a visible green-red band, related to a deep level defect emission, and an ultraviolet (UV) emission band originated from the ZnO excitonic emission [28,29]. Earlier studies suggest that the annealing of ZnO/AZO film improves the structure and light emission properties of the thin film.

With the increase of diabetic patients, glucose sensing is of paramount importance for the detection of glucose accurately and efficiently. Optical based techniques for glucose sensing are attractive due to its nondestructive and noninvasive nature [30–33]. Recently, ZnO nanostructures have been used for the sensitive detection of glucose by a non-destructive PL based quenching technique [30,34–36]. However, the nature of quenching has not been studied systematically. Further, there is no report on the use of AZO thin film for the sensitive detection of glucose using PL based optical technique.

In case of enzyme-conjugated sensor, the sensitive detection of biological molecules is associated with the PL quenching of a radiative material due to the charge transfer from the radiative material to a quencher (e.g., H_2O_2). Stern-Volmer plot of PL quenching of a fluorescent system can provide important information on the nature of the interaction between the fluorophore and the quencher (e.g., biological molecules), the selectivity and sensitivity of the sensor based on the fluorescence spectroscopy. Since efficient PL quenching of AZO thin film is highly desirable for a biomolecular sensor, it is imperative to understand the quenching mechanism.

In this article, we report on the growth of AZO thin films on Si substrate by a RF magnetron sputtering method using a high quality AZO target. As-grown films were annealed at different temperatures in a muffle furnace. The AZO thin film shows highly efficient visible PL before and after annealing, due to the intrinsic defects in ZnO. The post-growth annealing not only improves the structural quality of the AZO films, but also enhances the intensity of UV (~3.3 eV) and broad visible-NIR PL (1.6–2.2 eV) emission. The UV PL peak is originated from the near band edge emission of crystalline ZnO, while the broad visible-NIR peak is usually associated with the radiative transition related to oxygen interstitial (O_i) defects in the ZnO structure. The high intensity PL of the annealed samples was utilized for the label-free detection of glucose based on the PL quenching process. Our results show that AZO films can efficiently detect ~20 μM concentration of glucose in presence of glucose oxidase and the sensing follows a linear behaviour over a wide range of glucose concentrations (20 μM – 10 mM). We attempt to quantify, for the first time, the nature of PL quenching of AZO thin film in glucose-GOx medium using the standard Stern-Volmer plot. This enables us to quantify the sensing efficiency of AZO thin film and to explore the nature of interaction between the fluorophore and the quencher.

2. Experimental details

2.1. Deposition of AZO thin film

AZO thin films were grown on Si(100) and quartz substrates by RF magnetron sputtering at room temperature. At first, Si wafers and quartz substrates were cleaned by standard protocol and dried under Ar gas flow. Commercial AZO target (purity = 99.99%, Kurt J Lesker, USA) with ZnO:Al_2O_3 = 98:2 (wt%) was used for the growth of AZO thin films. We optimized the growth of AZO film by RF sputtering and found that a RF power of 100 W gives rise to reasonable deposition rate and good quality (polycrystalline) film. As-grown AZO thin films (Sample code, AZO) were thermally annealed in a muffle furnace at temperatures 250 °C, 450 °C and 650 °C for 1 h in air environment and the annealed samples are named as AZO250, AZO450 and AZO650, respectively.

2.2. Characterization techniques

The thickness of the AZO films was measured by a profilometer (Vecco, Dektak 150) and the thickness was found to be ~415 nm. The morphology and topography of AZO samples before and after annealing were characterized using a field emission scanning electron microcopy (FESEM, Sigma, Zeiss) and atomic force microscopy (AFM, Bruker). For structural characterizations, X-ray diffractometer (XRD) (Rigaku RINT 2500 TRAX–III, Cu Kα radiation) and an energy-dispersive X-ray spectrometer (EDX) were used. X-Ray photoelectron spectroscopy (XPS) measurements were carried out with a PHI X-Tool automated photoelectron spectrometer (PHI X-tool, ULVAC-PHI Inc.) using Al K_α X-ray beam (1486.6 eV) with a beam current of 5 mA. Carbon 1s spectrum (284.8 eV) was used for the calibration of the XPS spectra recorded for various samples [38]. XPS measurement was performed with a step size of 0.2 eV. The steady state PL spectrum of different samples was recorded using 355 nm and 405 nm diode lasers (CNI Laser) excitation with the help of a commercial fluorimeter (Horiba Jobin Yvon, Fluoromax-4). Raman scattering measurement was carried out with a 532 nm Ar laser excitation using a micro-Raman spectrometer (LabRAM HR-800, Jobin Yvon). UV–vis absorption spectra were recorded in a Shimadzu 2450 UV–vis spectrophotometer. Time resolved PL (TRPL) measurements were performed using a 405 nm pulsed laser excitation, with an instrument time response of <50 ps (LifeSpecII, Edinburgh Instruments).

2.3. Glucose sensing measurement

For the glucose sensing measurement, Glucose oxidase (GOx) from Aspergillus Niger (Sigma-Aldrich) in 0.01 M phosphate buffer solution (PBS, pH7) stock solution was prepared with concentration 2 mg/ml. Simultaneously, D-glucose (Merck) solutions with concentration 0.02, 0.05, 0.1, 0.2, 0.5, 1, 2, 4, 5, 7, 10 and 20 mM were prepared in PBS. 1 mL D-glucose solutions were mixed with 1 mL GOx solution in a 5 mL centrifuge tube and AZO samples (size ~8 × 8 mm^2) were dipped for 40 min in dark at room temperature. The samples were taken out and the sensing measurements were performed using a commercial fluorimeter (Horiba Jobin Yvon, Fluoromax-4) along with external laser excitation source (405 nm, 10 mW). PL intensity for each sample was measured at room temperature under identical conditions.

3. Results and discussion

3.1. Morphology and structural analysis

3.1.1. Atomic force microscopy (AFM)

AFM micrographs of AZO thin films on Si wafer before and after annealing (at 450 °C) are shown in Fig. 1(a) and (b), respectively. The corresponding line profiles are shown in Fig. 1(c) and (d), respectively. AFM confirms that the roughness of the sample is marginally increased and the average grain size is also increased after annealing. The RMS roughness of the as grown AZO sample is found to be 3.00 nm for a 2 × 2 μm^2 AFM image, while it is 3.05 nm for AZO450. Note that the shape of the grains is arbitrary and looks like “disc”, which is also confirmed from the FESEM analysis, as shown in Fig. S1(a) (as-grown sample) and S1(b) (annealed sample) (Supporting information).

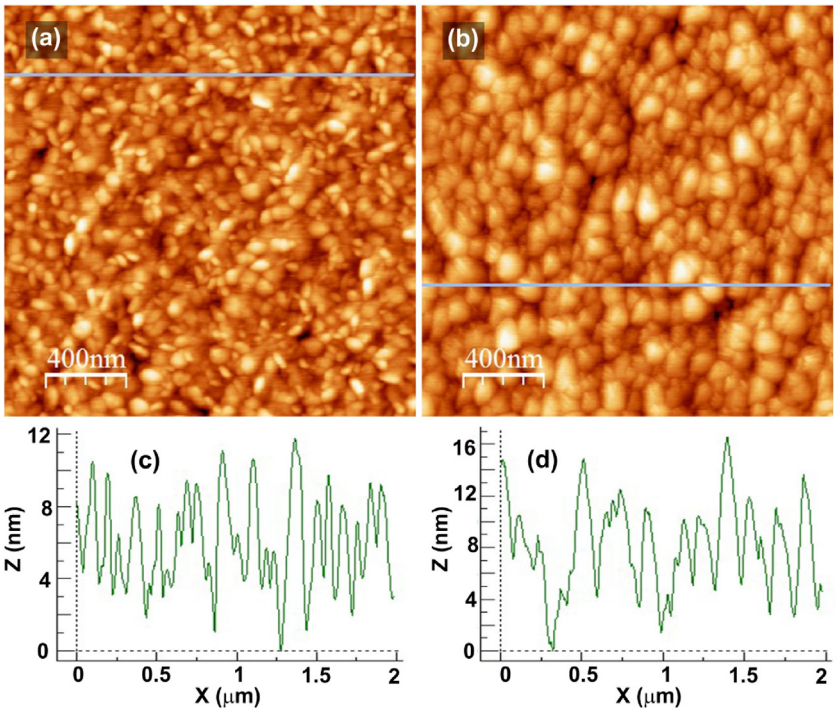

Fig. 1. AFM micrograph of sample AZO (a) before, and (b) after annealing at 450 °C. (c, d) The AFM height profile of the respective samples along the line shown in (a) and (b), respectively.

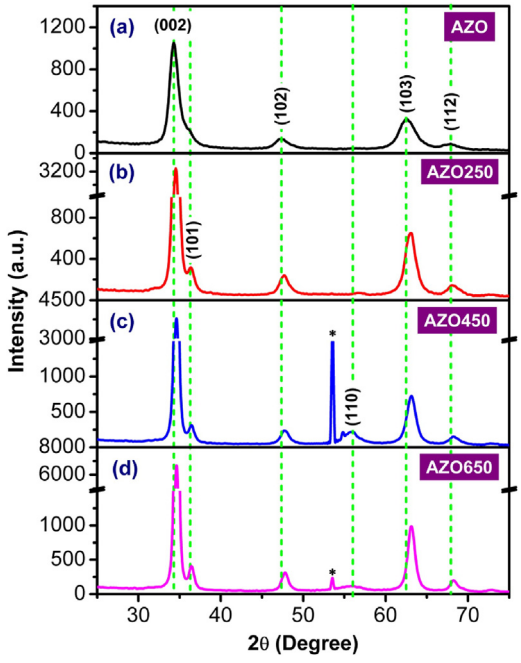

Fig. 2. XRD pattern of AZO samples before and after annealing at different temperatures: (a) AZO, (b) AZO250 (c) AZO450 (d) AZO650.

3.1.2. XRD analysis

A comparison of the XRD patterns of as-grown and annealed AZO samples processed at different temperatures are shown in Fig. 2(a–d). The different XRD peaks from different samples are distinguished and well matched with JCPDS database (Reference No. 80-0075). The XRD patterns of the samples indicate the hexagonal wurtzite ZnO phase with the space group of $P6_3mc$ (186). The EDX analysis of the sample AZO and AZO450 confirms the composition of crystalline AZO before and after annealing (Fig. S1(c) and (d), Supporting information). The peak positions are marked with dashed vertical lines in the figure. XRD pattern confirms that the films are polycrystalline in nature with preferred C-axis (002) orientation. The diffraction peak intensities increased systematically with increasing annealing temperature, indicating the improved crystallinity after annealing [39]. A careful analysis indicates that the XRD peaks of the annealed samples shifted slightly towards higher angle as compared to that of the as-grown AZO sample, and this shift towards the higher angle is systematic with the increase in annealing temperature. This is possibly due to the activation of some point defects and rearrangement of crystal grains [40]. The XRD pattern (Fig. 2(c) and (d)) of the sample annealed at temperatures 450 °C and 650 °C show additional peak at $2\theta = 53^\circ$ (marked *). Based on the JCPDS data, this peak is tentatively assigned to ZnO_2 phase (JCPDS reference no. 77-2414, 76-1364) [28]. This implies the enrichment of Oxygen species in the annealed samples. Note that the intensity of the Oxygen enriched peak is higher for the sample annealed at 450 °C as compared to that annealed at 650 °C. A clear view of the shift of (002) peak and enhancement of peak intensities are depicted in Fig. S2 (Supporting information). Corresponding full width at half maximum (FWHM) of the (002) peak for different samples are calculated after fitting considering the correction due to the instrumental broadening [41]. The crystallite sizes of different samples were calculated from (002) peak using Scherrer's formula:

$$D = \frac{k\lambda}{\beta cos\theta}, \quad (1)$$

where k is the Scherrer constant, λ is the wavelength of X-ray of Cu k_α-line (1.54 Å), β is the calculated FWHM and θ is the Bragg's angle. The calculated crystallite sizes of different samples are shown in Table 1. The average crystallite size is increased with the increase in annealing temperature, which is consistent with the AFM analysis.

3.1.3. XPS analysis

To investigate the chemical state and elemental composition, XPS analysis was performed on the as-grown and annealed AZO

Table 1
The FWHM and crystallite sizes of different AZO samples calculated from the XRD pattern corresponding to the (002) plane.

Samples	FWHM (degree)	Crystallite size (nm)
AZO	1.31	6.6
AZO250	0.73	11.9
AZO450	0.60	14.5
AZO650	0.50	17.4

thin films. All the peaks are calibrated by C1 s peak centered at ~284.8 eV [38]. Fig. 3(a) shows a comparison of the Zn 2p core level XPS spectra from sample AZO and AZO450. The peak at ~1021.7 eV corresponds to Zn $2p_{3/2}$ and the peak at ~1044.7 eV corresponds to Zn $2p_{1/2}$. The separation between Zn $2p_{3/2}$ (1021.7 eV) and Zn $2p_{1/2}$ (1044.7 eV) peak is shown by a blue arrow. An energy separation of 23.0 eV between two core level Zn 2p components makes out a good agreement with earlier published literature for crystalline ZnO [42]. Fig. 3(b) and (c) shows the XPS core level spectra of O1s from sample AZO and AZO450, respectively. The presence of Al in AZO samples is confirmed by Al 2p core level XPS spectra, as shown in Fig. S3 (Supporting information). However, the broad O1s spectra in each case of Fig. 3(a) and (b) confirm the presence of different oxidation states of ZnO. In order to understand the presence of Oxygen related defects and its nature, we have deconvoluted the O 1s spectrum in Fig. 3(b) and (c) by two Gaussian peaks. The 1st peak (Peak 1) centered at ~530.4 eV is attributed to the O^{2-} ions in wurtzite structure of a hexagonal Zn^{2+} ion array [40,43]. The 2nd peak (Peak 2) centered at ~531.8 eV corresponds to Oxygen-deficient regions within ZnO matrix, which is a signature of Oxygen vacancy (V_O) [44]. We have observed that the intensity of Peak 1 is unaltered after annealing, but that of Peak 2 is decreased. This strongly suggests that the concentration of V_O defect is decreased after annealing. Note that for sample AZO, the ratio of intensity of Peak 2 to Peak 1 is ~0.88, while it is ~0.75 in case of sample AZO450. This decrease in intensity ratio is the signature of reduced V_O after annealing [45]. This indirectly implies the oxygen enrichment in the annealed samples. From the XPS compositional analysis, we found that the O:Zn weight ratio is increased from 0.82 to 1.01 after annealing. This supports our assumption of the enrichment of oxygen content in the annealed samples. The Oxygen rich sites in annealed AZO samples have strong influence on the PL properties of the respective samples, as discussed later.

3.1.4. Micro-Raman analysis

Raman scattering is sensitive to the crystal lattice microstructure of AZO via its vibrational properties. In order to gather information concerning the crystallinity and phase of the AZO film, we have performed the micro-Raman measurement of the samples (on quartz substrates) before and after annealing. Fig. 4 shows a comparison of the Raman spectra of sample AZO and AZO450. The curves are vertically shifted for clarity of presentation. The Raman spectra of the AZO samples consist of peaks at wavenumbers (ω) ~101, 275, 450, 509 and 579 cm^{-1}, and the peak positions are marked by green dashed lines. Based on the literature, the observed Raman modes are assigned to standard modes of ZnO and depicted in Fig. 4. The modes at ω = 101 cm^{-1} and 450 cm^{-1} are doubly degenerate modes corresponding to E_2 (low) and E_2 (high), respectively [11]. The peak at ω = 579 cm^{-1} corresponds to A_1 (high) mode. The peak at ~580 cm^{-1} is believed to be associated with the intrinsic lattice defects and often it arises due to the doping [42]. The B_2 mode at ω = 275 cm^{-1} is observed for AZO films due to the built in electric dipole [46]. The presence of enhanced B_2 mode for the AZO samples also confirms the substitution of Zn by Al in ZnO structure. The mode at ω = 509 cm^{-1} is surface phonon mode (SPM), which is highly localized near the grain boundaries. The SPM peak is generally associated with the nanocrystalline particles [11]. The intensity of each Raman peak in AZO thin film is increased after annealing and it confirms the high crystalline structure in AZO450, which is consistent with the XRD analysis.

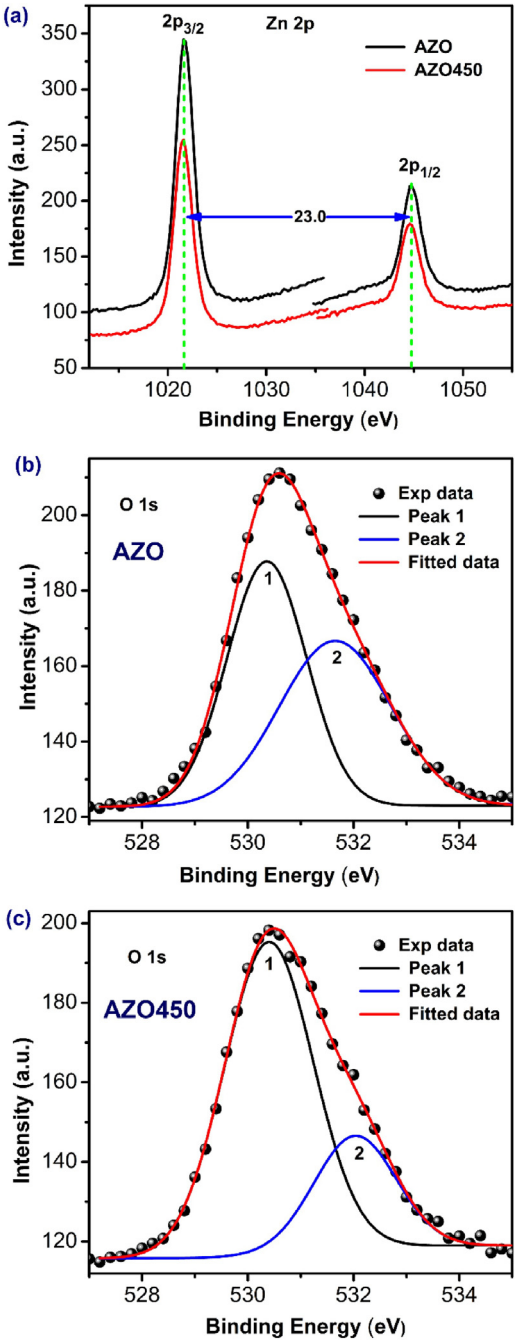

Fig. 3. (a) Comparison of Zn 2p core level XPS spectra of sample AZO and AZO450. The energy separation between the Zn $2p_{3/2}$ and Zn $2p_{1/2}$ peaks is shown by a blue arrow. (b, c) O1s XPS spectra of as-grown AZO film and AZO450, respectively. The symbols are the experimental data and the solid lines correspond to the fitted peaks. (For interpretation of the references to color in this figure legend, the reader is referred to the web version of this article.)

3.2. Optical properties

3.2.1. UV–visible absorbance study

We have investigated the UV–visible absorption characteristics of the samples and Fig. 5(a) shows the comparison of the absorbance spectra of the samples AZO and AZO450 in the range

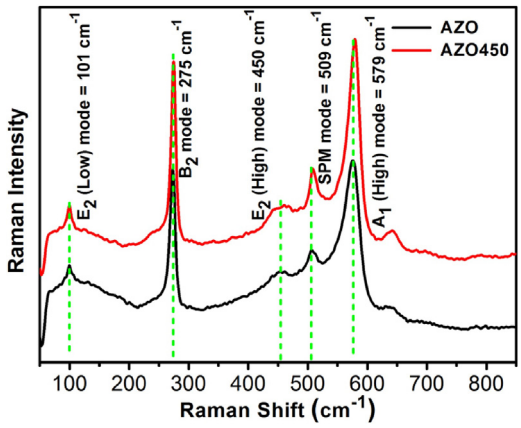

Fig. 4. Comparison of Raman spectra of as-grown AZO and annealed AZO450. The curves are vertically shifted to enable comparison. Peak centers are shown by the vertical dashed lines.

200–800 nm. It is evident that the absorbance of the sample AZO450 is enhanced both in the UV as well as the visible region as compared to that of AZO. The enhancement of absorbance in the visible region is mainly due to the increase in defect concentration that create deep levels in the band gap of ZnO and these are responsible for the enhancement of deep level emission (DLE) of the annealed samples (discussed later). The optical absorption can be used to determine the band gap of the material. The optical absorption coefficient, α, is determined using the following equation: $\alpha = 2.303\frac{A}{d}$, where, d is the thickness of the thin film and A is absorbance. Now, the band gap energy is calculated using the Tauc's eqn.

$$\alpha h\upsilon = C(h\upsilon - E_g)^n, \quad (2)$$

where C is constant, hν is the photon energy, E_g is the band gap energy and n is a number, which characterizes the transition process. Considering direct band gap nature of ZnO, we have plotted $(\alpha h\nu)^2$ *vs.* hν shown in Fig. 5(b) using the data shown in Fig. 5(a). The inset shows the enlarged view of the selected region. The optical band gaps of AZO and AZO450 have been estimated as 3.21 eV and 3.22 eV, respectively. Thus, no substantial change in bandgap is observed after annealing of the AZO films.

3.2.2. Photoluminescence study

Interestingly, the AZO thin films show highly efficient visible PL before and after thermal annealing. Fig. 6(a) shows a comparison of the visible PL spectra of the AZO before and after annealing. We have used a 405 nm diode pumped solid state (DPSS) laser for the excitation of the samples. The spectrum for each sample is broad and this broad PL is extended in the range 1.6–2.9 eV. This broad visible band is associated with deep level emissions (DLEs) due to intrinsic point defects and defect complexes in the AZO structure [8,17,28,29,47,48]. We observed that PL intensity of each sample is strongly enhanced after thermal annealing. In order to understand the origin of the broadband PL emission from the AZO samples and its enhancement after annealing, we have deconvoluted each spectrum by three Gaussian bands. Fig. 6(b) and (c) shows the deconvoluted PL spectra of the samples AZO and AZO450, respectively. The fitting shows that the spectrum in each case consists of three peaks: peak 1 at ~1.9 eV, peak 2 at ~2.2 eV and peak 3 at ~2.6 eV. According to the literature, the orange-red emission i.e. peak 1 (at ~1.9 eV) is attributed to the deep interstitial oxygen (O_i) states inside the AZO structures [8,17,48]; the yellowish-green emission, i.e. the peak 2 (at ~2.2 eV) is attributed to transition from the bottom of the conduction of AZO to the O_i states [28,29,49]; and the green emission i.e. peak 3 (~2.6 eV) is recognized as the V_O defects in the AZO structures [29,45,49]. Fig. 6(b) and (c) shows that the intensity of the orange-red emission, i.e., peak 1 is enhanced after annealing. This indicates that the density of O_i states is increased in AZO after annealing. This is fully consistent with the XRD and XPS analysis where we have observed an increase in oxygen content in the annealed samples as compared to that of the as-grown AZO sample. The ratio of the integrated intensity of peak 1 to peak 2 plus peak 3 is 1.2 for sample AZO, whereas it is 5.8 for the sample AZO450. According to Costas et al., the enhancement of the orange-red emissions in ZnO thin films after annealing is possibly due to the removal of non-radiative defects via thermal annealing, facilitating the radiative transfer associated with excess oxygen defects [8]. Interestingly, the PL results of AZO are similar to that of undoped ZnO. Note that we observed an enhanced PL after annealing for all the AZO samples. Fig. S4 (Supporting information) shows the UV PL spectra of the samples using 355 nm laser excitation. Each samples show a PL peak at ~3.33 eV (~376 nm) which is associated with the near band edge (NBE) emission of ZnO and it confirm the high crystalline quality of the AZO films. The increase in PL intensity of the NBE emission peak after annealing is possibly due to the improved crystallinity of ZnO, which is also confirmed from the XRD analysis. The high intensity visible-NIR PL of the sample AZO450 is utilized for the enzyme based glucose detection via fluorescence quenching process.

3.3. Glucose sensing

A simple approach to sensitive glucose detection has been developed based upon the variation in the fluorescence of semiconductor nanomaterials, such as CdSe/ZnS quantum dots (QDs) [50], Si QDs [51], CdTe QDs [32,52], ZnO NPs [34,35], ZnO NRs [30] etc. with glucose concentration in presence of a conjugate enzyme. Glucose oxidase (GOx) is stable, well-studied and widely used enzyme for glucose immobilization determination [30,32,34,35,50–52]. The

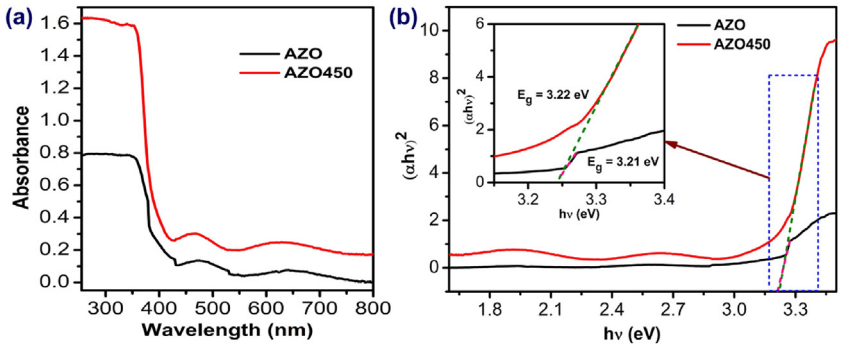

Fig. 5. (a) Comparison of the UV–vis absorbance spectra of samples AZO and AZO450. (b) The Corresponding Tauc plot, considering the direct bandgap nature of AZO. Inset shows the enlarged view of the selective portion to compare the band gap.

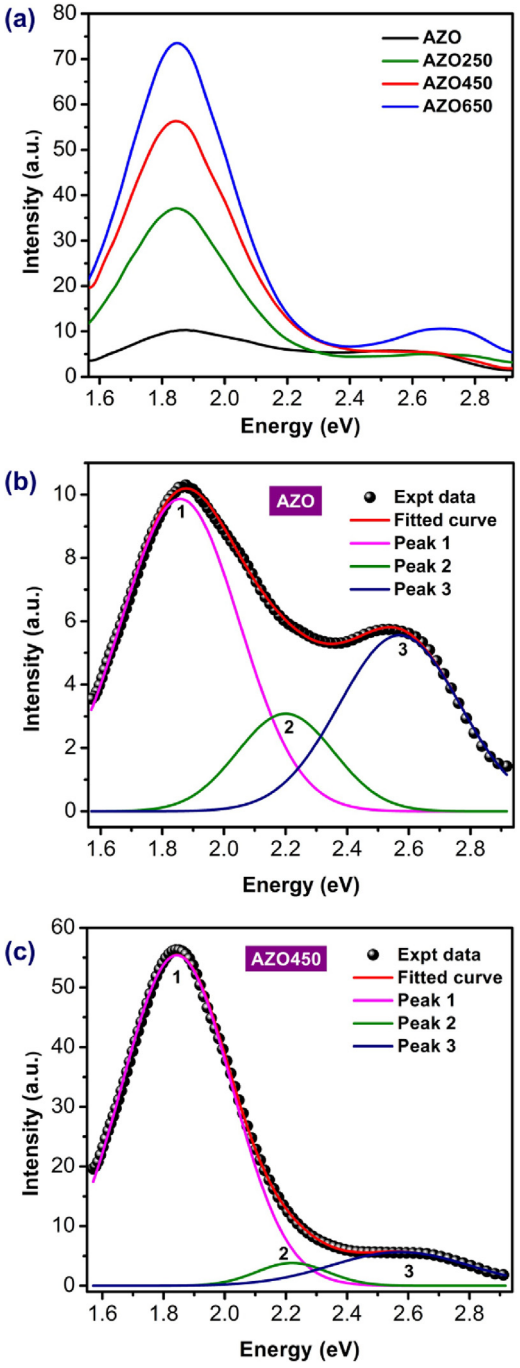

Fig. 6. (a) Comparison of the PL spectra of the as-grown and annealed AZO samples treated at different temperatures. The deconvoluted PL spectra of sample (b) AZO, and (c) AZO450 with 3 Gaussian bands (Peaks 1–3).

excellent specificity and high sensitivity of the ZnO nanostructures based fluorescence sensor suggest that the same technique might be directly applied for detecting glucose in the present case. Therefore, we investigated the label-free detection of D-glucose by the AZO samples based on the fluorescence quenching process. Fig. 7 shows the PL spectra of the sample AZO450 in presence of glucose at different concentrations and immobilized with GOx (as described in Section 2.3). The figure shows a systematic decrease in the PL intensity of AZO450 as the glucose concentration increases from 20 μM to 20 mM. The PL intensity as a function of glucose concentration is plotted in Fig. S5 (Supporting information) and at high glucose concentration it shows no substantial change in intensity.

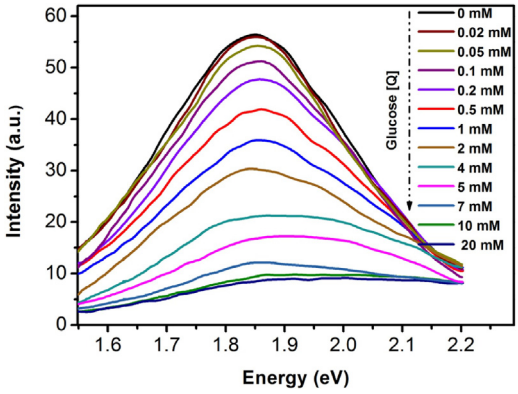

Fig. 7. PL spectra of sample AZO450 before and after glucose exposure at different concentrations in presence of GOx.

Note that we used the sample AZO450 for the fluorescence based glucose detection, since it shows best crystallinity among all the AZO samples annealed at different temperatures.

Several mechanisms have been proposed for the fluorescence quenching in presence of a quencher [30,32,34,35,50–53]. The surface reaction with a quencher may introduce nonradiative surface defects [30,32]. The charge transfer from a radiative material to a quencher was also proposed to be one of the possible mechanisms of the PL quenching in some studies [30,32]. Baratto et al. explained the PL quenching of ZnO NWs by the suppression of the radiative states [53]. In case of enzyme-conjugated sensor, H_2O_2 acts as a PL quencher based on the collisional quenching mechanism [30,32,34,35,50–52]. In the present case, the decrease in PL intensity is probably due to the presence of H_2O_2 which acts as a quencher. Note that the H_2O_2 is produced during the oxidation of the glucose molecules in presence of GOx.

For the confirmation of role of H_2O_2 in the PL quenching of AZO samples, we investigated the PL emission of the AZO samples before and after direct H_2O_2 treatment. Fig. 8(a) shows the PL quenching of the sample AZO450 in presence of H_2O_2 at different concentrations. As expected, the PL intensity of the sample AZO450 decreases systematically with the increase in H_2O_2 concentration. Collisional quenching may occur in this case when the excited-state fluorophore, AZO, is deactivated due to the contact with the quencher molecules in the solution, which is H_2O_2 in this case. During the photo-excitation process, the carriers in AZO are excited from the of deep level defects with energies ~1.6–2.2 eV and recombine radiatively by emitting photons, which is the cause of DLE PL. Due to the oxidation of glucose with GOx, H_2O_2 is produced and it decomposes catalytically on the AZO surface into H_2O and O_2. Since H_2O_2 can act as an electron acceptor, this reaction is accelerated by acceptance of electrons from the defect states of AZO, thus preventing its radiative recombination, and resulting in partial quenching of the PL emission intensity. The details of the carrier transfer mechanism from defect states of AZO to H_2O_2 are schematically illustrated in Fig. 8(b). In absence of the H_2O_2, radiative recombination of photoinduced e-h pairs in the defect sites of AZO is highly favourable, which results in high intensity visible PL form the AZO samples. On the other hand, in presence of the H_2O_2, recombination of photoinduced e-h pairs is less likely due to the transfer of electrons from defect state of AZO to H_2O_2 and hence the PL intensity of the AZO is reduced. For higher concentration of H_2O_2, the probability of recombination is lower; hence the PL intensity is lower.

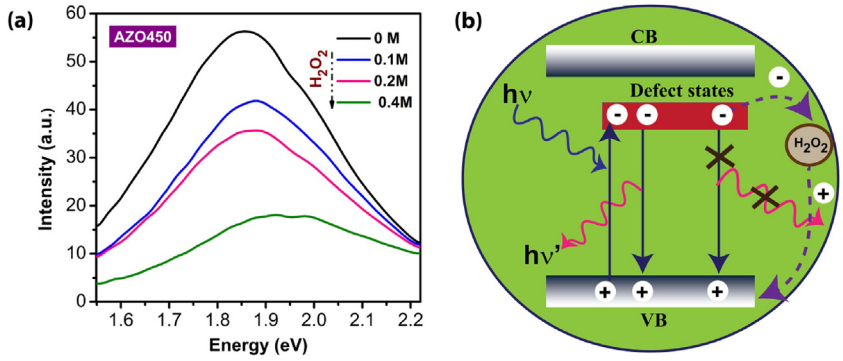

Fig. 8. (a) PL spectra of sample AZO450 before and after H_2O_2 exposure at different concentrations. (b) The schematic of the AZO-H_2O_2 interface, describing the photoinduced e-h pair separation and charge transfer mechanism.

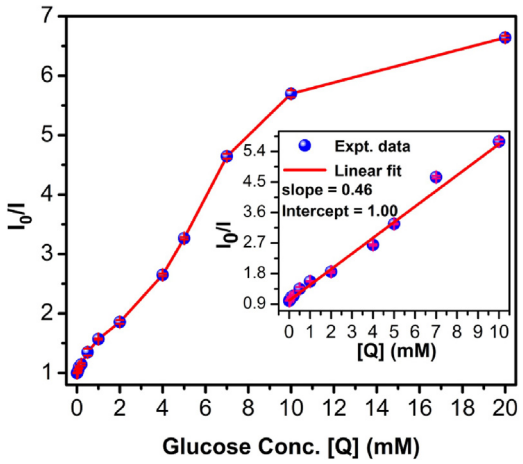

Fig. 9. Stern-Volmer plot for the sample AZO450 as function of glucose concentration. The inset shows the corresponding linear fit in the range 20 μM–10 mM.

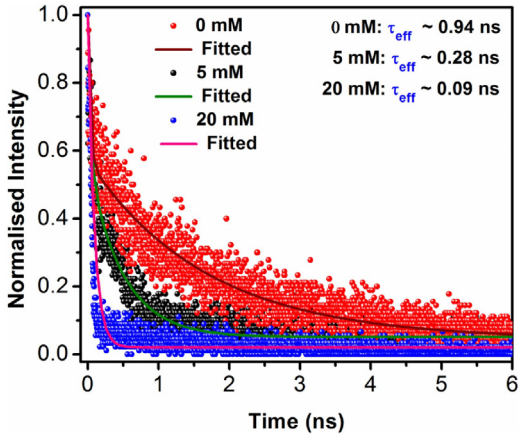

Fig. 10. Comparison of TRPL spectra of sample AZO450 before and after glucose exposure at different concentrations. The symbols are the experimental data and the solid lines are the corresponding bi-exponential fits. The effective time constants (τ_{eff}) are shown in the top-right corner.

The enzymatic oxidation of glucose produces D-gluconic acid and H_2O_2 where GOx acts as an oxidant in aqueous medium. The cyclic enzymatic reaction is as follows:

$$\text{Glucose} + O_2 + H_2O \overset{GOx}{\Rightarrow} \text{D-gluconic acid} + H_2O_2$$

The reaction between GOx and glucose is very specific. Wang et al. have shown that different sugars, such as fructose, sucrose and lactose hardly interfere on the detection of glucose, since GOx oxidizes glucose very specifically [54]. Note that H_2O_2 formation rate is directly proportional to the concentration of glucose. We have observed that the PL intensity of the sample AZO450 is decreased with increasing glucose concentration (Fig. 7).

In order to understand the nature of quenching, i.e. the relationship between the quenching effect (I_0/I) and glucose concentration, we have formulated the Stern–Volmer plot of the PL quenching for the sample AZO450. The quenching of PL intensity is quantitatively determined by the Stern-Volmer equation [55]:

$$\frac{I_0}{I} = 1 + K_{sv}[Q], \tag{3}$$

where I_0 is the PL intensity in absence of the quencher; I is the PL intensity in presence of the quencher, K_{SV} is the Stern-Volmer quenching constant and [Q] is the concentration of the quencher. Fig. 9 shows the Stern-Volmer plot for the sample AZO450 as a function of glucose concentration. Our data fits closely to a linear equation (Eq. (3)) with $K_{SV} = 0.46\ mM^{-1}$ and the intercept of 1.00, which shows the physical validity of the plot and the fitting. The inset of Fig. 9 shows the linear fit for the Stern-Volmer plot in the range 20 μM–10 mM concentration of glucose. The deviation of the data at higher concentration (>10 mM) arises possibly due to presence of both dynamic (electron transfer in this case) and static (ground state complex) quenching processes, while at low concentration of quencher, it follows solely a dynamic quenching (electron transfer) process [56]. In order to provide a direct evidence for the charge transfer mechanism, we have performed time resolved PL (TRPL) analysis of the sample AZO450 before and after glucose exposure at two different concentrations. The TRPL analysis shown in Fig. 10 clearly reveals that the effective time constant (τ_{eff}) decreases with increasing concentration of the quencher (glucose). Such behaviour is expected in case of dynamic quenching [55] and this is fully consistent with the charge transfer mechanism that causes the PL quenching.

Note that in the present case, we performed the experiment down to 20 μM concentration of glucose and the PL quenching was discernible to detect glucose efficiently in GOx medium by AZO. Thus, the sensitivity of our measurement is ~20 μM, which is comparable/better than the earlier reported data on the optical based glucose sensing by ZnO and other semiconductor nanostructures [37]. Table 2 shows a comparison of the performance of the AZO sensor with respect to other semiconductor nanostructures, which clearly displays the superiority of the AZO thin film as excellent glucose sensor [37]. In principle, the detection sensitivity can be much higher, depending on the sample and measurement conditions, and it can detect a concentration down to the nano-molar level, depending on the sensitivity of the spectrometer. Thus, it shows potential for the design of an optical biosensors for specific applications, e.g., glucose level in blood, food glucose control and

Table 2
Comparison of the glucose sensing performance of AZO thin film with other semiconducting materials/systems reported in the literature.

Sensing Additive	Sensing platform	Performance (detection limit/range)	Ref.
GOx	MUA capped ZnO nanoparticles	1.6–33.3 mM	[35]
GOx	ZnO nanoparticles	10–130 mM	[34]
GOx	CdTe quantum dots	0.5–16 mM	[32]
Non-enzymatic	ZnO nanorods	0.5–30 mM	[30]
GOx	Mn-doped ZnS quantum dots	10–100 μM	[33]
GOx	Al doped ZnO thin film	20 μM–20 mM	This study

environmental monitoring. Therefore, the further improvement of the sensing properties of the studied system may be investigated. The improvement in sensing efficiency of the AZO samples depends on several factors. These are: (i) improvement of the PL intensity of AZO films via defects incorporation; (b) optimization of different parameters, such as the concentration of GOx, reaction time and reaction temperature of the enzymatic reaction; (c) GOx immobilization procedure. We believe, our result will stimulate more detailed investigation for the further improvement of AZO thin film based biosensors.

4. Conclusions

We reported on the AZO thin film for the label-free detection of glucose based on the fluorescence quenching. We fabricated AZO thin films on Si and quartz substrates by the RF magnetron sputtering at room temperature. As compared to the as-grown AZO film, thermally annealed film showed improved structural and optical quality, which was confirmed from the XRD, XPS and Raman analyses. Besides the intrinsic UV PL, the as-grown and annealed samples exhibited broad visible-NIR PL, which was ascribed to the radiative transitions related to O_i defects in the AZO film. The PL peak intensity increased after annealing due to the removal of non-radiative defects and this high intensity PL of the annealed samples was utilized for the label-free enzyme-based detection of glucose. We achieved a very high sensitivity (20 μM) for the glucose detection in presence of GOx and the sensing mechanism was explained with the help of H_2O_2 based PL quenching of radiative fluorophore (AZO) via electron transfer mechanism from AZO to the quencher H_2O_2. A quantitative analysis of the PL quenching of AZO thin film in glucose-GOx medium has been made by the linear Stern-Volmer plot that provides the nature of the interaction between the fluorophore (AZO) and the glucose-GOx. This report may stimulate further investigation of AZO thin film and nanostructure for the non-destructive, label-free detection of glucose, cholesterol, ascorbic acid, lipids and other small molecules with high sensitivity and selectivity.

Acknowledgements

We acknowledge the financial support from CSIR (Grant No. 03(1270)/13/EMR-II) and DEITY (Grant No. 5(9)/2012-NANO(VOL-II)) for carrying out part of this work. Central Instruments Facility, IIT Guwahati is acknowledged for the FESEM and Raman facilities. We also acknowledge Prof. Fujii, Kobe University, for the XPS measurement.

Appendix A. Supplementary data

Supplementary data associated with this article can be found, in the online version, at http://dx.doi.org/10.1016/j.snb.2017.07.110.

References

[1] S. Dhara, P.K. Giri, Stable p-type conductivity and enhanced photoconductivity from nitrogen-doped annealed ZnO thin film, Thin Solid Films 520 (2012) 5000.
[2] M. Law, L.E. Greene, J.C. Johnson, R. Saykally, P. Yang, Nanowire dye-sensitized solar cells, Nat. Mater. 4 (2005) 455.
[3] D.-K. Hwang, S.-H. Kang, J.-H. Lim, E.-J. Yang, J.-Y. Oh, J.-H. Yang, S.-J. Park, p-ZnO/n-GaN heterostructure ZnO light-emitting diodes, Appl. Phys. Lett. 86 (2005) 222101.
[4] D.-Y. Guo, C.-X. Shan, S.-N. Qu, D.-Z. Shen, Highly sensitive ultraviolet photodetectors fabricated from ZnO quantum dots/carbon nanodots hybrid films, Sci. Rep. 4 (2014) 7469.
[5] S. Dhara, P.K. Giri, ZnO/anthracene based inorganic/organic nanowire heterostructure: photoresponse and photoluminescence studies, J. Appl. Phys. 111 (2012) 044320.
[6] F. Fleischhaker, V. Wloka, I. Hennig, ZnO based field-effect transistors (FETs): solution-processable at low temperatures on flexible substrates, J. Mater. Chem. 20 (2010) 6622.
[7] H. Zeng, W. Cai, P. Liu, X. Xu, H. Zhou, C. Klingshirn, H. Kalt, ZnO-based hollow nanoparticles by selective etching: elimination and reconstruction of metal-semiconductor interface, improvement of blue emission and photocatalysis, ACS Nano 2 (2008) 1661.
[8] T. Costas, C. Wayne, L. Flora, A. Khairi, F. Andrew, K. Demosthenes, R. Robert, Intrinsic photoluminescence from low temperature deposited zinc oxide thin films as a function of laser and thermal annealing, J. Phys. D: Appl. Phys. 46 (2013) 095305.
[9] V.L. Patil, S.A. Vanalakar, P.S. Patil, J.H. Kim, Fabrication of nanostructured ZnO thin films based NO2 gas sensor via SILAR technique, Sens. Actuators B Chem. 239 (2017) 1185–1193.
[10] N.H. Al-Hardan, M.J. Abdullah, A.A. Aziz, Sensing mechanism of hydrogen gas sensor based on RF-sputtered ZnO thin films, Int. J. Hydrogen Energy 35 (2010) 4428–4434.
[11] N. Srinatha, Y.S. No, V.B. Kamble, S. Chakravarty, N. Suriyamurthy, B. Angadi, A.M. Umarji, W.K. Choi, Effect of RF power on the structural, optical and gas sensing properties of RF-sputtered Al doped ZnO thin films, RSC Adv. 6 (2016) 9779.
[12] P.P. Sahay, R.K. Nath, Al-doped zinc oxide thin films for liquid petroleum gas (LPG) sensors, Sens. Actuator B-Chem. 133 (2008) 222.
[13] K. Jindal, M. Tomar, V. Gupta, Nitrogen-doped zinc oxide thin films biosensor for determination of uric acid, Analyst 138 (2013) 4353–4362.
[14] S.K. Arya, S. Saha, J.E. Ramirez-Vick, V. Gupta, S. Bhansali, S.P. Singh, Recent advances in ZnO nanostructures and thin films for biosensor applications: review, Anal. Chim. Acta 737 (2012) 1–21.
[15] K. Muthukrishnan, M. Vanaraja, S. Boomadevi, R.K. Karn, V. Singh, P.K. Singh, K. Pandiyan, Studies on acetone sensing characteristics of ZnO thin film prepared by sol-gel dip coating, J. Alloys Compd. 673 (2016) 138–143.
[16] N. Akin, U. Ceren Baskose, B. Kinaci, M. Cakmak, S. Ozcelik, AZO thin film-based UV sensors: effects of RF power on the films, Appl. Phys. A 119 (2015) 965–970.
[17] L. Castañeda, O.G. Morales-Saavedra, J.C. Cheang-Wong, D.R. Acosta, J.G. Bañuelos, A. Maldonado, M.L. d. l. Olvera, Influence of indium concentration and substrate temperature on the physical characteristics of chemically sprayed ZnO: in thin films deposited from zinc pentanedionate and indium sulfate, J. Phys. Condens. Matter 18 (2006) 5105.
[18] Q. Li, X. Li, J. Zhang, Microstructure, optical and electrical properties of gallium-doped ZnO films prepared by so-gel method, J. Alloy Compd. 572 (2013) 175.
[19] K. Huang, Z. Tang, L. Zhang, J. Yu, J. Lv, X. Liu, F. Liu, Preparation and characterization of Mg-doped ZnO thin films by sol?gel method, Appl. Surface Sci. 258 (2012) 3710.
[20] R.N. Moussawi, D. Patra, Modification of nanostructured ZnO surfaces with curcumin: fluorescence-based sensing for arsenic and improving arsenic removal by ZnO, RSC Adv. 6 (2016) 17256–17268.
[21] R.N. Moussawi, D. Patra, Nanoparticle self-assembled grain like curcumin conjugated ZnO: curcumin conjugation enhances removal of perylene, fluoranthene, and chrysene by ZnO, Sci. Rep. (2016) 24565.
[22] M. Mouslmani, D. Patra, Modifying emission of ZnO nanoparticles in ZnO interceded polymer based hierarchical ordered nanocapsules, Mater. Lett. 143 (2015) 135–139.

[23] A.E. Manouni, F.J. Manjón, M. Mollar, B. Marí, R. Gómez, M.C. López, J.R. Ramos-Barrado, Effect of aluminium doping on zinc oxide thin films grown by spray pyrolysis, Superlattices Microstruct. 39 (2006) 185.
[24] S.H. Jeong, J.W. Lee, S.B. Lee, J.H. Boo, Deposition of aluminum-doped zinc oxide films by RF magnetron sputtering and study of their structural, electrical and optical properties, Thin Solid Films 435 (2003) 78.
[25] Y.J. Wu, Y.S. Wei, C.Y. Hsieh, P.M. Lee, C.H. Liao, Y.S. Liu, C.Y. Liu, Preparation of V-doped AZO thin films and ZnO nanorods on V-doped AZO thin films by hydrothermal process, J. Sol-Gel Sci. Technol. 73 (2015) 647–654.
[26] N. Koshizaki, T. Oyama, Sensing characteristics of ZnO-based NOx sensor, Sens. Actuator B-Chem. 66 (2000) 119.
[27] Y.S. No, D.H. Park, T.W. Kim, J.W. Choi, B. Angadi, W.K. Choi, Enhancement of electrical properties in Al-doped ZnO films by tuning dc bias voltage during radio frequency magnetron sputtering, Curr. Appl. Phys. 12 (2012) S71–S75.
[28] R. Ghosh, P.K. Giri, K. Imakita, M. Fujii, Photoluminescence signature of resonant energy transfer in ZnO coated Si nanocrystals decorated on vertical Si nanowires array, J. Alloy Compd. 638 (2015) 419.
[29] B. Lin, Z. Fu, Y. Jia, Green luminescent center in undoped zinc oxide films deposited on silicon substrates, Appl. Phys. Lett. 79 (2001) 943.
[30] S.N. Sarangi, S. Nozaki, S.N. Sahu, ZnO nanorod-based non-enzymatic optical glucose biosensor, J. Biomed. Nanotechnol. 11 (2015) 988.
[31] R. Ghosh, P.K. Giri, Silicon nanowire heterostructures for advanced energy and environmental applications: a review, Nanotechnology 28 (2017) 012001.
[32] X. Li, Y. Zhou, Z. Zheng, X. Yue, Z. Dai, S. Liu, Z. Tang, Glucose biosensor based on nanocomposite films of CdTe quantum dots and glucose oxidase, Langmuir 25 (2009) 6580.
[33] P. Wu, Y. He, H.-F. Wang, X.-P. Yan, Conjugation of glucose oxidase onto Mn-doped ZnS quantum dots for phosphorescent sensing of glucose in biological fluids, Anal. Chem. 82 (2010) 1427–1433.
[34] D. Sodzel, V. Khranovskyy, V. Beni, A.P.F. Turner, R. Viter, M.O. Eriksson, P.-O. Holtz, J.-M. Janot, M. Bechelany, S. Balme, V. Smyntyna, E. Kolesneva, L. Dubovskaya, I. Volotovski, A. Ubelis, R. Yakimova, Continuous sensing of hydrogen peroxide and glucose via quenching of the UV and visible luminescence of ZnO nanoparticles, Microchim. Acta. 182 (2015) 1819.
[35] K.E. Kim, T.G. Kim, Y.-M. Sung, Enzyme-conjugated ZnO nanocrystals for collisional quenching-based glucose sensing, CrystEngComm 14 (2012) 2859.
[36] S. Elhag, Z.H. Ibupoto, V. Khranovskyy, M. Willander, O. Nur, Habit-modifying additives and their morphological consequences on photoluminescence and glucose sensing properties of ZnO nanostructures, grown via aqueous chemical synthesis, Vacuum 116 (2015) 21–26.
[37] A. Tereshchenko, M. Bechelany, R. Viter, V. Khranovskyy, V. Smyntyna, N. Starodub, R. Yakimova, Optical biosensors based on ZnO nanostructures: advantages and perspectives. A review, Sens. Actuators B: Chem. 229 (2016) 664–677.
[38] R. Ghosh, K. Imakita, M. Fujii, P.K. Giri, Effect of Ag/Au bilayer assisted etching on the strongly enhanced photoluminescence and visible light photocatalysis by Si nanowire arrays, Phys. Chem. Chem. Phys. 18 (2016) 7715.
[39] X.J. Liu, C. Song, F. Zeng, X.B. Wang, F. Pan, Influence of annealing on microstructure and magnetic properties of co-sputtered Co-doped ZnO thin films, J. Phys. D: Appl. Phys. 40 (2007) 1608.
[40] U. Ilyas, R.S. Rawat, T.L. Tan, P. Lee, R. Chen, H.D. Sun, L. Fengji, S. Zhang, Oxygen rich p-type ZnO thin films using wet chemical route with enhanced carrier concentration by temperature-dependent tuning of acceptor defects, J. Appl. Phys. 110 (2011) 093522.
[41] G. Rajender, P.K. Giri, Strain induced phase formation, microstructural evolution and bandgap narrowing in strained TiO2 nanocrystals grown by ball milling, J. Alloy Compd. 676 (2016) 591.
[42] K. Mahmood, S.B. Park, H.J. Sung, Enhanced photoluminescence, Raman spectra and field-emission behavior of indium-doped ZnO nanostructures, J. Mater. Chem. C (2013) 3138.
[43] J. Wang, Z. Wang, B. Huang, Y. Ma, Y. Liu, X. Qin, X. Zhang, Y. Dai, Oxygen vacancy induced band-gap narrowing and enhanced visible light photocatalytic activity of ZnO, ACS Appl. Mater. Int. 4 (2012) 4024.
[44] X. Li, X. Cao, L. Xu, L. Liu, Y. Wang, C. Meng, Z. Wang, High dielectric constant in Al-doped ZnO ceramics using high-pressure treated powders, J. Alloy Compd. 657 (2016) 90.
[45] D. Das, P. Mondal, Photoluminescence phenomena prevailing in c-axis oriented intrinsic ZnO thin films prepared by RF magnetron sputtering, RSC Adv. 4 (2014) 35735.
[46] M. Tzolov, N. Tzenov, D. Dimova-Malinovska, M. Kalitzova, C. Pizzuto, G. Vitali, G. Zollo, I. Ivanov, Vibrational properties and structure of undoped and Al-doped ZnO films deposited by RF magnetron sputtering, Thin Solid Films 379 (2000) 28.
[47] S.A. Studenikin, N. Golego, M. Cocivera, Fabrication of green, orange photoluminescent, undoped ZnO films using spray pyrolysis, J. Appl. Phys. 84 (1998) 2287–2294.
[48] Y.G. Wang, S.P. Lau, X.H. Zhang, H.W. Lee, H.H. Hng, B.K. Tay, Observations of nitrogen-related photoluminescence bands from nitrogen-doped ZnO films, J. Cryst. Growth 252 (2003) 265.
[49] S. Dhara, P.K. Giri, On the origin of enhanced photoconduction and photoluminescence from Au and Ti nanoparticles decorated aligned ZnO nanowire heterostructures, J. Appl. Phys. 110 (2011) 124317.
[50] W.C.W. Chan, S. Nie, Quantum dot bioconjugates for ultrasensitive nonisotopic detection, Science 281 (1998) 2016.
[51] Y. Yi, J. Deng, Y. Zhang, H. Li, S. Yao, Label-free Si quantum dots as photoluminescence probes for glucose detection, Chem. Comm. 49 (2013) 612.
[52] J. Yuan, W. Guo, J. Yin, E. Wang, Glutathione-capped, CdTe quantum dots for the sensitive detection of glucose, Talanta 77 (2009) 1858.
[53] C. Baratto, S. Todros, G. Faglia, E. Comini, G. Sberveglieri, S. Lettieri, L. Santamaria, P. Maddalena, Luminescence response of ZnO nanowires to gas adsorption, Sens. Actuators B: Chem. 140 (2009) 461.
[54] G.-L. Wang, X.-L. Hu, X.-M. Wu, Z.-J. Li, Quantum dots-based glucose sensing through fluorescence quenching by bienzyme-catalyzed chromogenic substrate oxidation, Sens. Actuators B: Chem. 205 (2014) 61–66.
[55] D.K. Singh, P.K. Iyer, P.K. Giri, Role of molecular interactions and structural defects in the efficient fluorescence quenching by carbon nanotubes, Carbon 50 (2012) 4495.
[56] D. Patra, N.N. Malaeb, Fluorescence modulation of 1,7-bis(4-hydroxy-3-methoxyphenyl)-1,6-heptadiene-3,5-dione by silver nanoparticles and its possible analytical application, Luminescence 27 (2012) 11–15.

Biographies

Joydip Ghosh graduated (B.Sc. Hons in Physics) from the University of Kalyani in 2013 and obtained his Masters degree in Physics from Banaras Hindu University in 2015. Presently he is a PhD scholar at the Department of Physics, Indian Institute of Technology Guwahati, and he is working in the area of inorganic-organic hybrid perovskite solar cells and thin films for photovoltaics and sensor applications.

Ramesh Ghosh obtained his Bachelors and Masters degree in Physics both from Visva-Bharati University in 2007and 2009, respectively. He obtained his PhD degree in Physics from the Department of Physics, Indian Institute of Technology Guwahati in 2017 and he is currently working on Semiconductor nanowire/thin film based biosensors and solar cells.

P. K. Giri obtained his PhD in Physics from Indian Institute of Technology Kanpur in 1998 and then moved to Italy for postdoctoral research with ICTP TRIL fellowship. During 1999–2001, he worked in Indira Gandhi Centre for Atomic Research, Kalpakkam as a Scientist. Later he moved to Indian Institute of Technology Guwahati as an Assistant Professor of Physics. Presently he is a full Professor of Physics and Center for Nanotechnology at the same institute. For his outstanding research contributions, he received several national/international awards/fellowships including ICTP TRIL fellowship (1998), DAE Young Scientist Award (2000), DAAD Exchange visit Fellowship (2010), JSPS Invitation Fellowship for log-term research in Japan (2012) etc. He has published 115 Research articles including 5 review articles in high profile international journals and holds 01 Patent to his credit. He is an Executive Council Member of Electron Microscopy Society of India. His research areas of interests are semiconductor nanostructures, optoelectronics, 2D Materials based hybrid nanostructures for energy and environmental applications, nanobiosensors, etc.